

## Mechanical model for seismic response assessment of lightly reinforced concrete walls

E. Brunesi<sup>\*1</sup>, R. Nascimbene<sup>1a</sup> and A. Pavese<sup>2b</sup>

<sup>1</sup>*EUCENTRE, European Centre for Training and Research in Earthquake Engineering  
Via Ferrata 1, 27100 Pavia (PV), Italy*

<sup>2</sup>*Department of Civil Engineering and Architecture, University of Pavia  
Via Ferrata 3, 27100 Pavia, Italy*

*(Received September 18, 2015, Revised September 6, 2016, Accepted September 7, 2016)*

**Abstract.** The research described in this paper investigates the seismic behaviour of lightly reinforced concrete (RC) bearing sandwich panels, heavily conditioned by shear deformation. A numerical model has been prepared, within an open source finite element (FE) platform, to simulate the experimental response of this emerging structural system, whose squat-type geometry affects performance and failure mode. Calibration of this equivalent mechanical model, consisting of a group of regularly spaced vertical elements in combination with a layer of nonlinear springs, which represent the cyclic behaviour of concrete and steel, has been conducted by means of a series of pseudo-static cyclic tests performed on single full-scale prototypes with or without openings. Both cantilevered and fixed-end shear walls have been analyzed.

After validation, this numerical procedure, including cyclic-related mechanisms, such as buckling and subsequent slippage of reinforcing re-bars, as well as concrete crushing at the base of the wall, has been used to assess the capacity of two- and three-dimensional low- to mid-rise box-type buildings and, hence, to estimate their strength reduction factors, on the basis of conventional pushover analyses.

**Keywords:** lightweight concrete wall; shear wall; sandwich panel; finite element model; multi-spring model; seismic response; strength reduction factor

### 1. Introduction

Over the last few decades, the use of shotcrete sandwich panels as lateral-force resisting system of low- to mid-rise buildings has become a quite common practice in many countries, due to more than known advantages, such as fast and economic construction, consistent reduction of self-weight and high thermal and acoustic performance. Even though these solutions are still not explicitly certified to be used in any major building specification jurisdiction, intensive large-scale experimental programs (Salonikios *et al.* 1999, 2000, Hidalgo *et al.* 2002, Rezaifar *et al.* 2008, Dazio *et al.* 2009, Pavese and Bournas 2011, Palermo *et al.* 2013, 2014, Ricci *et al.* 2013, Mousavi

---

\*Corresponding author, Ph.D., E-mail: [emanuele.brunesi@eucentre.it](mailto:emanuele.brunesi@eucentre.it)

<sup>a</sup>Ph.D., E-mail: [roberto.nascimbene@eucentre.it](mailto:roberto.nascimbene@eucentre.it)

<sup>b</sup>Ph.D., E-mail: [a.pavese@unipv.it](mailto:a.pavese@unipv.it)

*et al.* 2014, Zygouris *et al.* 2015) have been carried out, showing their significant potential for load-bearing capacity. Both quasi-static and shaking-table tests on full-scale single panels and more complex building layouts have revealed a promising structural response characterized by valuable overstrength and ductility reserves for strong earthquake excitations. For such precast or cast-in place systems, the key role played by a proper design and detailing of the joints is well-established in the literature (Belleri and Riva 2012, Belleri *et al.* 2015, Brunesi *et al.* 2015a, 2015b). Redundant wall-to-wall and wall-to-slab connections may ensure a bundled-tube behaviour (Pavese and Bournas 2011, Palermo *et al.* 2014, Mousavi *et al.* 2014), thus mitigating the effects of lightweight low-strength concretes. In fact, the high redundancy of such box-type structures results into stress peaks lower and less concentrated than those experienced in traditional RC frames, which conversely present limited paths for gravity and seismic load transfer (Mousavi *et al.* 2014).

Besides extensive experimental efforts, the seismic behaviour of this construction technology has not been deeply explored from a numerical point of view. Few research contributions (Mousavi *et al.* 2014, Miao *et al.* 2006, Werasak and Jing 2009) have proposed accurate but time consuming high-definition FE models, using bricks with constitutive laws based on classical principles of nonlinear fracture mechanics (Bruggi 2009, Hung and El-Tawil 2010, Pecce *et al.* 2014, Brunesi *et al.* 2015a, c, Brunesi and Nascimbene 2015) and multi-layered shell elements with prevented locking phenomena and spurious energy modes (Nascimbene and Venini 2002, Nascimbene 2014). In particular, a specific energy-based isotropic continuum damage model has been recently integrated with the latter element formulation for seismic analysis of similar panels (Palermo and Trombetti 2016). Even though these advanced computational techniques may give some more insight than equivalent mechanical models, the computational time tremendously increases, asking necessarily advantage of parallel processing on multiprocessor computers and, in addition, making this representation almost unfeasible if the response of a whole building has to be investigated. By contrast, fiber-based approaches combined with nonlinear zero-length elements are usually attractive solutions to incorporate complex phenomena into modern structural analysis programs, thus predicting the global response of whole structures and structural subassemblies in a simplified but time saving way (Brunesi *et al.* 2014, 2015d). Different sources of geometric and material nonlinearities can be taken into account and several studies (Brunesi *et al.* 2015e, 2016, Arshian *et al.* 2016) have demonstrated the applicability of fiber-beam based solutions for damage analysis of structures, considering either earthquake-induced loads or other low probability-high consequence events that can be simulated in both static and dynamic fashion. Also, the versatility and multipurpose potential of this element type render it applicable for numerical modeling of soil-structure interaction problems with explicit consideration of foundation flexibility and site-specific effects (Saad *et al.* 2016).

In light of this scenario, one of the main objectives of this study is to develop a quick modeling procedure for large-scale nonlinear static analysis of three-dimensional building configurations, combining Bernoulli beam and multi-spring elements with the open platform OpenSees (McKenna *et al.* 2015). Examples of full-scale lightly reinforced concrete shear walls, tested in a past program (Pavese and Bournas 2011), have been numerically analyzed and their response compared with experimental observations, in order to quantify the effectiveness of the proposed approach. Then, a series of conventional pushover analyses have been performed on a building stock, consisting of two- and three-dimensional layouts representative of the construction technique studied. Based on these results, a simplified methodology (Miranda and Bertero 1994) has been implemented to conservatively estimate the strength reduction factors of structures built with this

particular technology.

## 2. Experimental investigation

Details concerning test setup and procedure, as well as a brief description of specimens, materials and reinforcement layouts, will be summarized in the following. Further information regarding the experimental campaign of pseudo-static cyclic tests, assumed as reference in this work, can be found in Pavese and Bournas (2011).

### 2.1 Description of test specimens

The solution investigated consists of an expanded polystyrene foam core with prefabricated steel wire mesh reinforcement encased in two layers of sprayed concrete on both sides, as shown in Fig. 1, where a schematic of this composite technology, with its key components, is provided.

In detail, the ten reference specimens, whose main characteristics are detailed in Table 1, were 3×3 m or 4×3 m panel prototypes (with or without door or window), composed of an intermediate

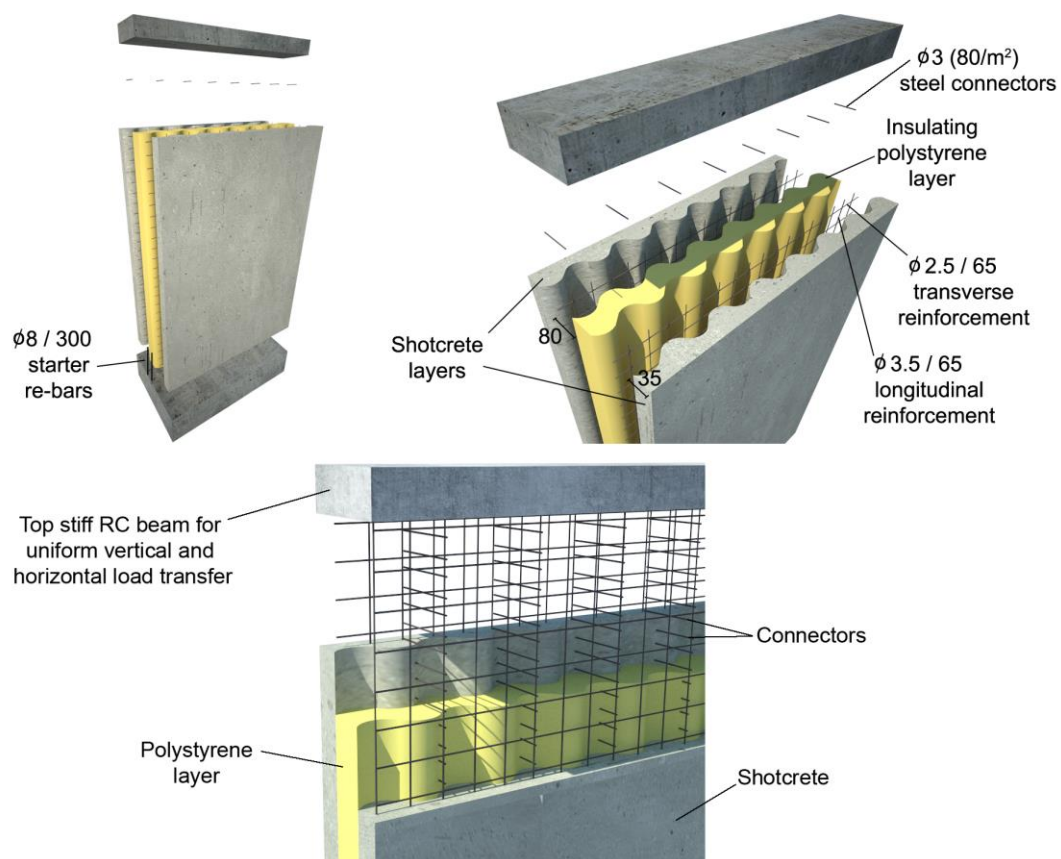


Fig. 1 Construction technology: details of a typical lightweight lightly reinforced shotcrete sandwich panel. Note: dimensions are in mm

Table 1 Characteristics of the experimental prototypes: geometry, boundary condition and axial load

Specimen	Dimension	Opening	Testing condition	Axial load
01	3×3 m	None	Single bending	150 kN - 2.5%
02	3×3 m	None	Single bending	300 kN - 5.0%
03	3×3 m	Door (0.9×2.1 m)	Single bending	150 kN - 2.5%
04	3×3 m	Door (0.9×2.1 m)	Single bending	300 kN - 5.0%
05	3×3 m	Window (1.2×1.2 m)	Single bending	150 kN - 2.5%
06	3×3 m	Window (1.2×1.2 m)	Single bending	300 kN - 5.0%
07	4×3 m	None	Single bending	150 kN - 1.9%
08	4×3 m	None	Single bending	300 kN - 3.8%
09	3×3 m	None	Double bending	150 kN - 2.5%
10	3×3 m	None	Double bending	300 kN - 5.0%

80 mm thick corrugated thermal insulating sheet and two 35 mm thick shotcrete layers, reinforced by means of a 65×65 mm hot-galvanized grid of Ø3.5 vertical and Ø2.5 horizontal bars. To couple the two RC layers, a series (~80/m<sup>2</sup>) of Ø3 straight steel connectors were welded to the front and back wire meshes through the polystyrene. Traditional mild steel, with a nominal yielding stress of 600 MPa, was used for both mechanical couplers and mesh reinforcement, while the characteristic 28-days cube compressive strength of the shotcrete was measured to be higher than 25 MPa. The foundation was post-tensioned to the strong floor of the lab to inhibit any uplift and to simulate a rigid connection to the soil. The panel-to-foundation connection was implemented through Ø8 starter re-bars, spaced of 300 mm. A reinforced concrete beam was provided on the top of the wall to permit a uniform application of both vertical and horizontal load paths during the experimental test. The panel-to-top beam connection was developed using the same re-bars distribution adopted for the panel-to-foundation case.

## 2.2 Test setup and procedure

The ten full-scale sandwich panels were tested under cyclic in-plane flexure with a constant axial load, corresponding approximately to 2.5% and 5.0% of their compressive strength, in single or double bending. A quasi-static cyclic displacement history at increasing top displacement levels was imposed by a horizontal MTS actuator, in displacement control. In particular, the experimental loading protocol consisted of a series of five symmetric horizontal top drift targets as reported in Table 2; three cycles per amplitude were planned. The axial load was applied through a couple of hydraulic jacks, acting on the top concrete beam and post-tensioned to the concrete block at the base of the wall. In double bending configuration, a set of two vertical MTS actuators, in a combined force and displacement control mode, was used to keep the total axial load constant and fix the rotation of the top beam to zero.

Fig. 2 shows a schematic of test setup and instrumentation. A series of linear variable differential transformers (LVDTs) were used to measure absolute and relative quantities at key locations throughout the specimen. In detail, the LVDTs were arranged to monitor displacements at different levels up to the height of the panel, its flexural and shear deformations, base uplift and slippage in the concrete footing.

Table 2 Experimental loading protocol: imposed drift levels for each prototype

Specimen type	
1, 2, 3, 4, 5, 6, 7, 8	9, 10
Drift level [%]	
± 0.10	± 0.10
± 0.20	± 0.20
± 0.40	± 0.40
± 0.60	± 0.80
± 1.00	± 1.00

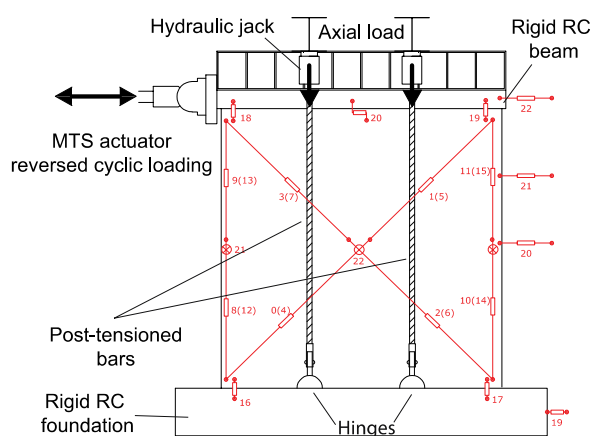


Fig. 2 Schematic of test setup and instrumentation

### 3. Nonlinear FE analyses of full-scale specimens

To reproduce the experimental behaviour of the specimens tested at Eucentre laboratory (Pavese and Bournas 2011), an equivalent mechanical model, consisting of a set of infinitely stiff vertical elastic elements in combination with a layer of nonlinear springs, has been constructed in OpenSees code (McKenna *et al.* 2015) and, hence, a series of geometrically and materially nonlinear FE simulations have been performed to validate the numerical approach proposed to study the response of this structural system, at a global scale. In the following, the prevailing characteristics and assumptions related to this FE idealization will be described and discussed. Furthermore, a direct comparison will be provided between experimental and numerical base shear-top displacement curves in order to quantify the effectiveness of FE predictions. Finally, numerical curves will be compared to outline behavioural changes in load-bearing capacity and global displacement ductility as a consequence of axial load increments and variations in the geometry (i.e., wall depth and presence of openings) of these panels, acting as membrane elements (i.e., in-plane shear and axial stresses).

#### 3.1 Numerical representation

In Fig. 3, a schematic of the planar representation prepared for seismic response assessment of

these lightweight sandwich panels can be observed. Elastic Bernoulli beam-column elements, uniformly spaced of 250 mm, have been introduced to materialize the geometry of the wall and then, they have been rigidly connected to each other at the top and bottom of the specimen using a series of rigidLink objects (McKenna *et al.* 2015). A one-to-one correspondence has been assumed between structural portions of the panel and model elements along the height. Very high stiffness has been assigned to these members, thus creating a sort of macro-rigid block floating on a multi-spring element used to lump equivalent nonlinear material properties (Colotti 1993, Ghobarah and Youssef 1999, Orakcal *et al.* 2004, 2009), as discussed later on. Scale factors equal to  $10^3$  have been adopted to amplify the elastic properties of the panel and penalty coefficients equal to  $10^{14}$  have been consistently selected to avoid numerical instability. Further and more specific details concerning the classical penalty method assumed herein can be found in McKenna *et al.* (2015). A one-to-one correspondence between vertical rigid and zero-length elements has been adopted to impose a spring-to-spring gap able to capture the neutral axis elongation (Priestley *et al.* 1999), as done in similar numerical models for controlled multi-rocking systems (Kurama *et al.* 1999, Kurama 2000, Pennucci *et al.* 2009).

Geometric nonlinearity has been accounted using a classical co-rotational transformation, whose implementation is based on an exact description of the kinematic transformations associated with large displacements and rotations of the members (Brunesi and Nascimbene 2014). Material nonlinearity has been described by a discrete approach, in which the sectional stress-strain state of the wall is obtained through the integration of the uniaxial stress-strain response of the individual springs at its base. As done by Brunesi and Nascimbene (2014), the classical uniaxial uniform confinement model proposed by Mander *et al.* (1988) and modified according to Chang and Mander (1994) (i.e., Material Concrete07) has been used to represent concrete behaviour, accounting for tension softening, while a bi-linear idealization (i.e., Material Steel01), has been assumed for steel.

Hence, the tributary area of concrete and steel has been computed for each zero-length element and the contribution of the two materials has been assembled in parallel to define the flexural behaviour of the specimen, which is reproduced, in a phenomenological sense, by the tensile and compressive forces developed along the axial component of each spring. Flexural and shear

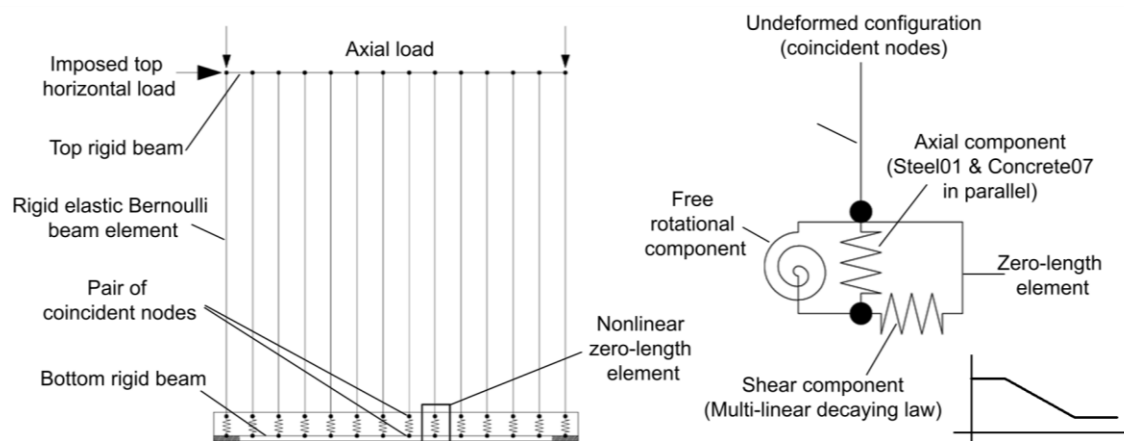


Fig. 3 FE representation for experimental response assessment

mechanisms have been decoupled and the latter has been concentrated in the transverse component of each spring, by an equivalent multi-linear constitutive law, calibrated in accordance with experimental observations by Pavese and Bournas (2011). In addition, the rotational component of this equivalent multi-spring element has been assumed to add no contribution to the response of such wall systems and, hence, its elastic stiffness has been assigned accordingly. Finally, insulating polystyrene layers have been omitted in the simulations performed, being conservatively assumed to provide any further bearing capacity against seismic loads. The prevailing assumptions introduced for the calibration of this equivalent discrete approach will be specified hereafter.

### *3.2 Assumptions and accuracy of FE predictions*

As it is intended to be used for monotonic analyses, this mechanical model has been calibrated to include cyclic-related mechanisms, such as concrete crushing at wall base and buckling/slippage of reinforcing re-bars, into an equivalent manner. Fig. 4 presents an example of concrete spalling and crushing observed during tests (i.e., Specimen 01 - see Table 1 for its characteristics). In particular, cracking initially takes place at the concrete cover, in correspondence to the compressed edge of the wall, because of the buckling in compression of the reinforcing bars protruding from the foundation. As a result, they are no longer able to fully grip concrete and mesh reinforcement, when the specimen is loaded in the opposite direction during cyclic reversals, and, hence, relative slippage partially occurs. Even though the nature of loading causes this behaviour to manifest itself during cyclic FE analyses and experimental tests, a monotonic simulation evidences the need for an equivalent way to account for this mechanism.

In accordance with experimental observations, an approximately 15-20 cm wide portion of the wall was affected by such damage pattern, which progressively develops along the base and, therefore, peculiar softening stress-strain relationships have been implemented in the springs at the corners of the specimen. A linearly decaying post-yielding branch, which becomes zero at a local



Fig. 4 Concrete (a) spalling and (b) crushing in compression (Specimen 01)

ductility level equal to 8, has been introduced to model the behaviour of the steel re-bars, while the damage of concrete has been simulated by scaling its compressive strength to roughly a quarter of the average resistance measured from compressive cylinder tests. Peak stress has been assumed to occur at a strain level of  $1 \cdot 10^{-3}$ , while a value of  $2 \cdot 10^{-3}$  has been imposed as the ultimate concrete strain at which the compressive stress goes to zero.

As suggested by Beyer *et al.* (2008), the elastic properties of the transverse springs have been computed to represent the shear stiffness of uncracked sections in which the shear area was taken as 80% of the gross area. The model proposed by Priestley *et al.* (1994) has been considered to include a potential nonlinear behaviour in shear, by means of a tri-linear constitutive law, consisting of two constant branches and an intermediate linearly decaying relationship between shear strength and ductility. Its calibration has been done in accordance with the decomposition of the total wall displacement into flexural and shear deformations given in Pavese and Bournas (2011).

A displacement/rotation-based convergence criterion, with a threshold set equal to  $10^{-3}$ , has been used to equilibrate loads through an incremental iterative procedure; Newton-Raphson has been assumed to play out the simulations collected in Fig. 5, where a comparison is provided between numerical monotonic estimates and experimental curves from cyclic tests.

Quite accurate predictions have been obtained in terms of peak base shear, while the discrepancy between numerical and experimental data tends to increase, as the lateral displacement imposed increases and damage propagates into the panel up to the final buckling of the reinforcing re-bars. Yielding has been observed to occur at drifts in the range 0.19-0.26%, while their peak shear force developed at drifts approximately ranging from 0.39% to 0.60%. To identify the collapse occurrence, conventional performance criteria have been defined in terms of strain limits for concrete and steel and their first exceedance has been assumed as a conservative check of the “near collapse” limit state. In particular, a value of  $5 \cdot 10^{-3}$  has been selected as the ultimate concrete compressive strain, accounting for the confinement effect provided by the transverse reinforcement (Mander *et al.* 1988), and a value of  $6 \cdot 10^{-2}$  has been fixed as the ultimate steel strain. Hence, the specimens analyzed have experienced conventional failure at drifts in the range 0.45-1.00%, thus resulting into global displacement ductility levels of about 2.1-4.5.

Table 3 provides a summary of the experimentally observed ( $V_{obs}$ ) and numerically predicted ( $V_{pre}$ ) maximum base shear. In addition, their ratios ( $R_i$ ) have been computed and shown herein, revealing a satisfying agreement between numerical and experimental estimates:  $0.908 < R_i < 1.016$ , with an average of 0.973 and a moderate standard deviation roughly equal to 4%. As shown in Fig. 6, an even more accurate match has been achieved, whether only specimens without openings (i.e., 01, 02, 07, 08, 09, 10) are considered, since the average of  $R_i$  is close to unity (i.e., 1.001), with an almost negligible standard deviation (i.e., 1.3%). By contrast, the accuracy of this approach decreases in case of prototypes presenting doors and windows (i.e., 03, 04, 05, 06); compared to the experimental results, a mismatch of about 7% is determined, in average, with a standard deviation of 2.3%.

In single bending configuration, the numerical idealization proposed is effective in equivalently reproducing the formation and propagation of shear cracks parallel to the compression strut, as well as the significant longitudinal and horizontal tensile cracks developed close to the zones of maximum moment (see Fig. 7), lumping them at the base of the specimens. An approximately 17% increase in peak base shear has been observed, doubling the imposed axial load (i.e., Specimen 02 vs. 01 and 08 vs. 07), while a 25% elongation of wall depth resulted in a roughly 39% higher maximum lateral force (07 vs. 01 and 08 vs. 02). In addition, a 37% stiffer capacity curve has

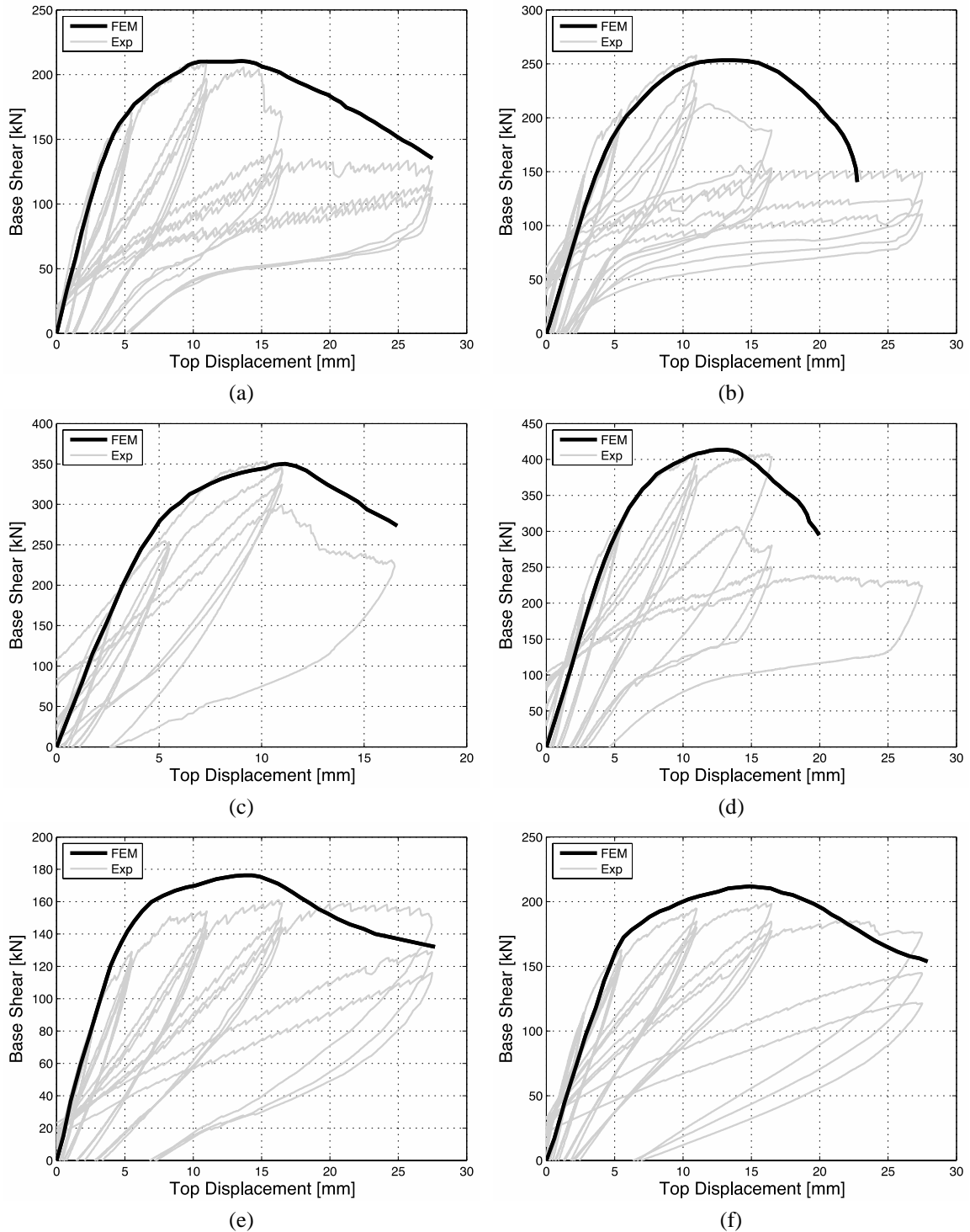
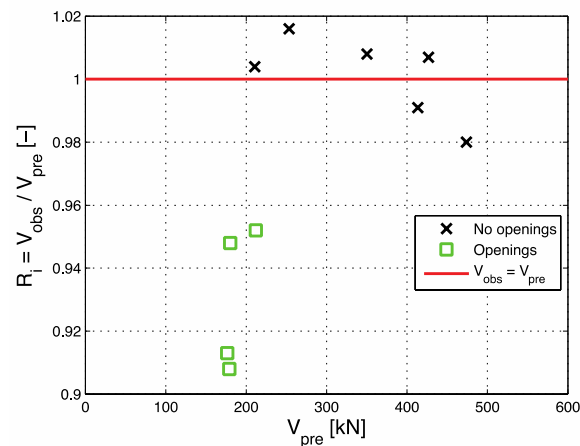


Fig. 5 Numerical vs. experimental estimates: (a) Specimen 01; (b) Specimen 02; (c) Specimen 07; (d) Specimen 08; (e) Specimen 03 and (f) Specimen 06, respectively

Table 3 Experimentally observed ( $V_{obs}$ ) vs. numerically predicted ( $V_{pre}$ ) maximum base shear

Specimen	$V_{obs}$ [kN]	$V_{pre}$ [kN]	$R_i = V_{obs}/V_{pre}$
01	211.4	210.6	1.004
02	257.4	253.4	1.016
03	160.9	176.3	0.913
04	162.6	179.1	0.908
05	170.8	180.2	0.948
06	201.8	212.0	0.952
07	352.9	350.2	1.008
08	409.8	413.4	0.991
09	429.7	426.8	1.007
10	464.5	473.8	0.980
<b>Avg.</b>			0.973
<b>St. Dev.</b>			0.040

Fig. 6  $V_{obs}/V_{pre}$  vs.  $V_{pre}$  for each reference prototype

been predicted. Similarly, the adoption of a double bending condition implied a more rigid response, dominated by shear due to a quite low value of the shear span ratio. In this case, a strong coupling between flexure and shear has been observed; after flexural yielding at the corner of the specimen, sliding shear failure occurred as a consequence of slightly buckled longitudinal bars working as a dowel reinforcement. As a result, Specimen 09 and 10 revealed capacity 45-50% higher than those assessed in single bending configuration (i.e., 01 and 02). Furthermore, a less pronounced (i.e., 10%) increase in peak base shear has been determined, doubling the axial load applied (see Fig. 8).

As presented in Fig. 9, a displacement-based fiber element has been placed at the center line of the lintel; the depth of its cross-section equals the height of the lintel and the width equals the thickness of the wall. A similar approach has been used for Specimen 05 and 06, introducing an additional element under the window. In this case, the model is able to capture the formation of

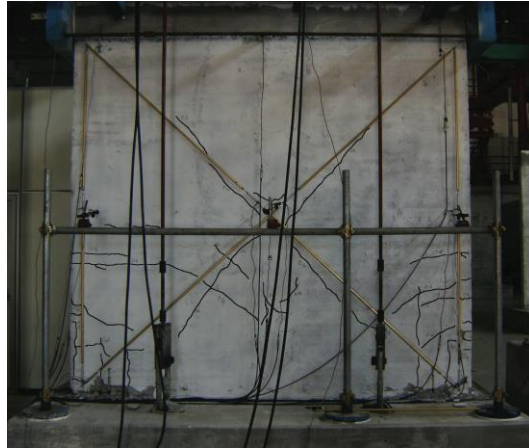


Fig. 7 Example of experimentally observed horizontal, vertical and shear cracks

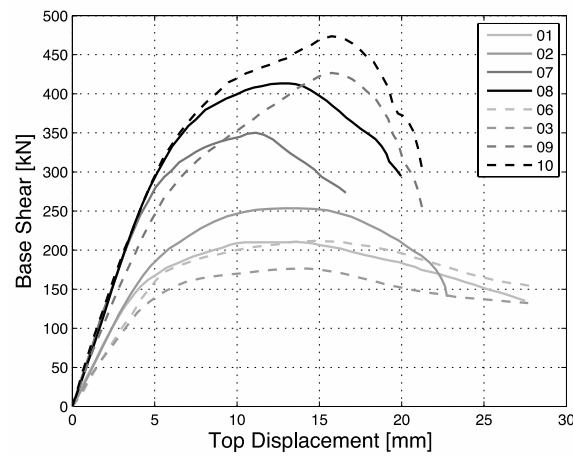


Fig. 8 Comparison between lateral load-top displacement capacity curves

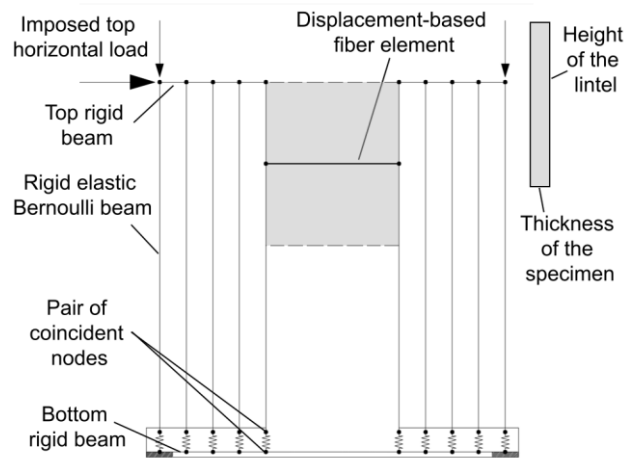


Fig. 9 Proposed numerical idealization in case of openings (Specimen 03 and 04)



Fig. 10 Damage at the corners of the openings (i.e., door and window)

initial shear cracks at the base and the stiffness reduction caused by the presence of windows or doors, but it slightly overestimates the peak strength, being unable to reproduce damage in correspondence to the corners of the openings (see Fig. 10). By contrast, this representation is quite effective in simulating the post-peak branch, characterized by a relatively gradual and regular strength and stiffness degradation induced by the appearance of several flexural cracks after maximum lateral load, due to the response of the two parts of the panel as individual walls, with a larger shear span ratio, which favours higher flexural deformation.

#### 4. Seismic response assessment of box-type building prototypes

Once it was quantified its effectiveness in compliance with experimental observations, the equivalent mechanical model proposed herein has been adopted for seismic response assessment of practical real-life examples of structural prototypes built with this particular construction technique. It is well-known that nonlinear time history analysis is usually a favourite numerical approach for performance evaluation, collapse simulation and design verification of structures, as it can take into account the physical nature of earthquake excitation in terms of dynamic effects and propagation of damage during cyclic loading. Despite this, analysis results are ground motion-sensitive and high computational costs are necessarily required to determine reliable estimates with an acceptable level of confidence. No unanimous consensus has been yet achieved on a unique procedure for selecting and scaling or matching accelerograms to obtain a compatible suite of records, while several research works (Miranda and Bertero 1994, Krawinkler and Seneviratna 1998, Kim and D'Amore 1999, Fajfar 2000, Chopra and Goel 2002, Antoniou and Pinho 2004) have proven the feasibility of traditional and more recent nonlinear static methods of analysis as a robust alternative, showing that higher levels of complexity and numerical efforts are not straightforwardly associated with higher accuracy, particularly in the case of standard low- and mid-rise structural systems. Hence, a series of conventional static pushover analyses have been performed on the reference buildings detailed in the following, in order to estimate their force

reduction factor ( $R_q$ ), according to the procedure reported by Miranda and Bertero (1994).

#### 4.1 Reference structural layouts

The panels numerically analyzed in the previous section have been assembled to compose five reference layouts, whose geometry agrees with conventional characteristics used by the producer for residential/office buildings. A schematic of plan view and three-dimensional representation of these systems is provided in Fig. 11, while their main features are summarized in Table 4.

Type 1, 2 and 3 consist of  $2 \times 1$  blocks, composed of  $3 \times 3$  m<sup>2</sup> span systems, but they present different percentages of openings (see Fig. 11). Type 4 consists of  $2 \times 3$  blocks, composed of two

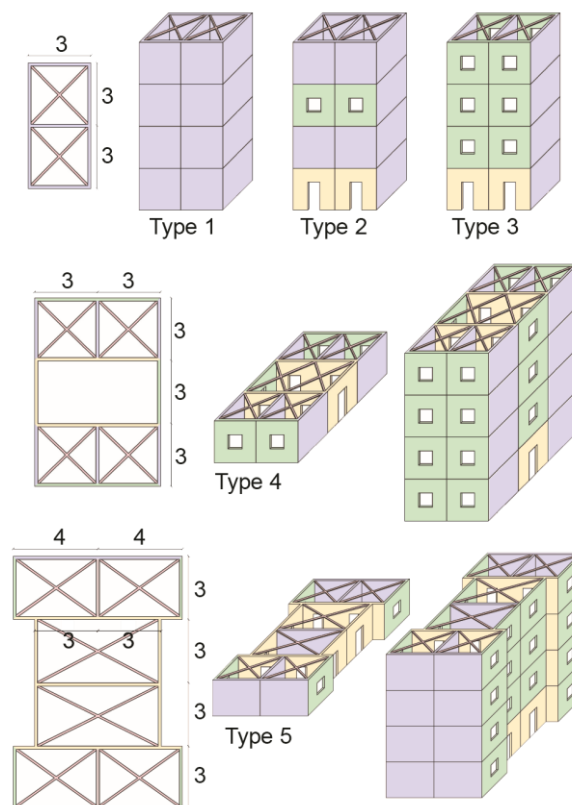


Fig. 11 Geometry of the reference structural layouts

Table 4 Reference building typologies: nomenclature, geometrical characteristics and analysis direction

Type	Blocks	Floor span	$n_f$	Openings	Direction
1	$2 \times 1$	$3 \times 3$ m <sup>2</sup>	1 - 4	NO	L
2	$2 \times 1$	$3 \times 3$ m <sup>2</sup>	1 - 4	YES	L
3	$2 \times 1$	$3 \times 3$ m <sup>2</sup>	1 - 4	YES	L
4	$2 \times 3$	$3 \times 3$ - $6 \times 3$ m <sup>2</sup>	1 - 4	YES	L & S
5	$2 \times 4$	$4 \times 3$ - $6 \times 3$ m <sup>2</sup>	1 - 4	YES	L & S

3×3 m<sup>2</sup> span systems at its edges and an intermediate 6×3 m<sup>2</sup> span block. Finally, Type 5 consists of 2×4 blocks, composed of two 4×3 m<sup>2</sup> span systems at its edges and two inner 6×3 m<sup>2</sup> span systems.

The inter-storey height is considered to be constant and equal to 3 m, according to the geometry of the walls tested. For each structural typology, the number of floors ( $n_f$ ) is selected to vary from 1 to 4. A one-way slab is assumed to distribute dead and live loads, which are assigned to simulate the normalized axial load levels imposed during the tests. Its weight and inertia are implicitly included in the numerical simulations, concentrating them at the top of each panel. Equivalent linear elastic diagonal trusses are introduced, concentrating both flexural and shear stiffness of the slab into the axial properties of those elements.

#### 4.2 Force reduction factor (FRF) estimates: results and discussion

The methodology implemented in this study to obtain the FRFs presented in the upcoming discussion has been synthesized in Fig. 12. For each building typology, a linear elastic analysis and a conventional nonlinear static analysis have been carried out, applying an inverted triangular lateral force distribution, and then  $R_q$  has been computed as the ratio between the base shear determined from the two simulation techniques, at a conventionally fixed displacement level. In particular, two values have been selected, according to the following criteria:

- 1) The lateral displacement ( $\Delta_{peak}$ ) that corresponds to the attainment of the peak strength;
- 2) The lateral displacement ( $\Delta_{0.4\%}$ ) that corresponds to the attainment of an inter-storey drift of 0.4%, which was proven, either experimentally or numerically, to anticipate major damage in such lightweight lightly reinforced concrete sandwich panels.

In this latter case, a bilinear idealization has been constructed to calculate  $R_q$ , imposing the 75% and 90% of the maximum force experienced during nonlinear analyses to identify the nominal yielding of the system. Therefore, Figs. 13 and 14 collect the base shear-top displacement capacity curves predicted by the series of displacement-controlled nonlinear pushover analyses conducted, while Fig. 15 systematically presents the capacity curves of each building in terms of normalized base shear (i.e., base shear/building seismic weight) versus roof drift (i.e., roof displacement/total building height).

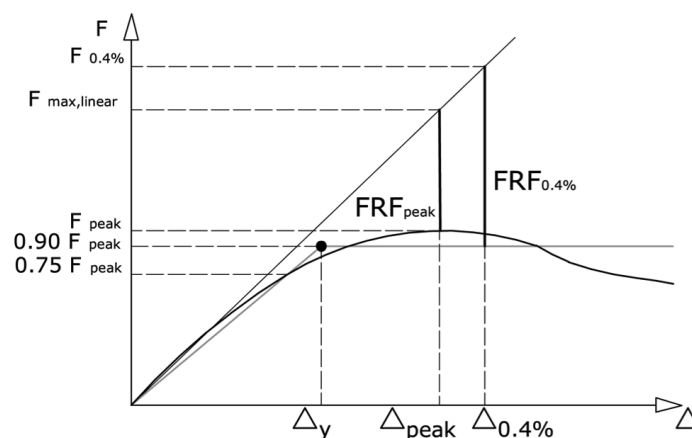


Fig. 12 Conceptual scheme of the procedure implemented for FRF estimates

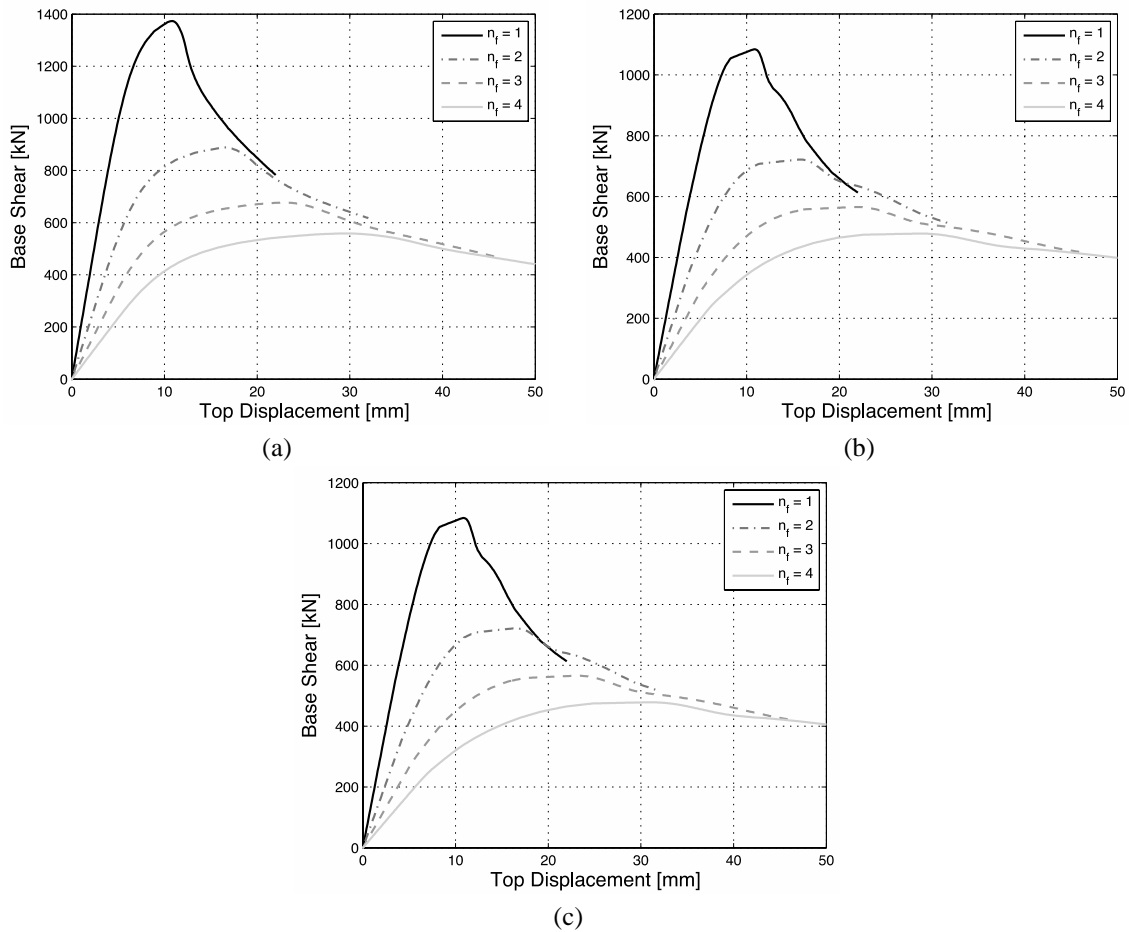


Fig. 13 Base shear-roof displacement curves for (a) Type 1; (b) Type 2 and (c) Type 3, respectively

Second, third and fourth floor level additions result into an approximately 46%, 37% and 33% less stiff response - 2<sup>nd</sup> vs. 1<sup>st</sup>, 3<sup>rd</sup> vs. 2<sup>nd</sup> and 4<sup>th</sup> vs. 3<sup>rd</sup>, respectively; this reduction refers to Type 1, but a similar trend has been observed for the other case-studies. In terms of peak strength, one more floor level implies a 35%, 24% and 17% decrease for Type 1, while slightly lower percentages (i.e., 33%, 22% and 15%) have been computed in case of Type 2 and 3. For Type 4 and 5, both short (S) and long (L) directions have been analyzed and Type 4 has shown a smaller reduction in the former case (i.e., S-direction), while an opposite trend has been evidenced for Type 5, because of its less regular configuration in plan: 31%, 20% and 16% vs. 34%, 23% and 17%, when Type 4 is referred, and 31%, 21% and 16% vs. 30%, 20% and 17%, if Type 5 is considered. In the majority of the cases, a more regular and smoother post-peak path is predicted, as the number of floors increases. A similar consideration can be drawn in case that normalized pushover curves are concerned (see Fig. 15).

Finally, Fig. 16(a) and (b) summarize the set of FRFs obtained for any structural type and height considered. The sensitivity of  $R_q$  to this parameter directly arises from the considerations previously drawn in terms of stiffness and strength reduction with increasing  $n_f$ . The FRF is

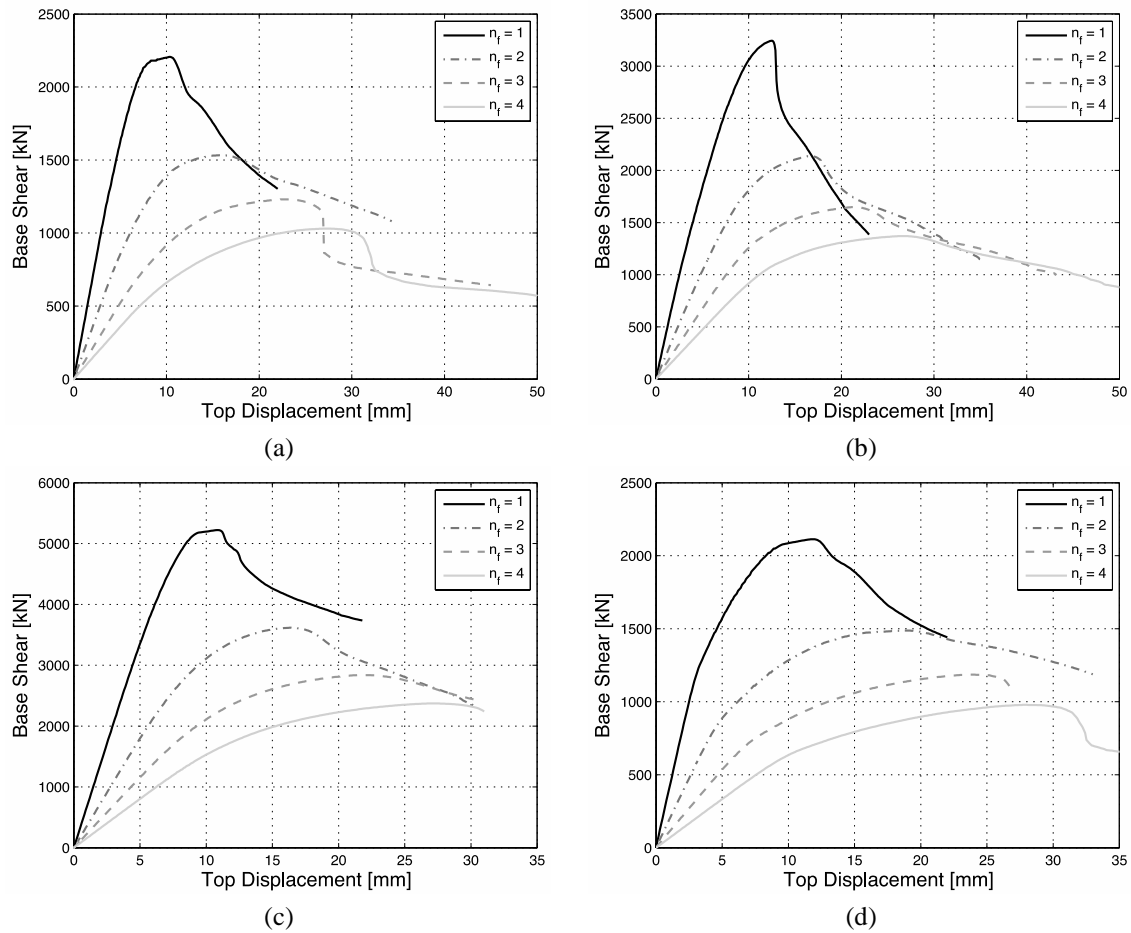


Fig. 14 Base shear-roof displacement curves for (a) Type 4S; (b) Type 4L; (c) Type 5S and (d) Type 5L, respectively. Note: S and L stand for short- and long-direction of the building prototypes

confirmed to increase, as the height of the building increases (see Fig. 16), particularly for regular structures. Criterion 2) leads to strength reduction factors of up to 20-50% larger than those determined by assuming criterion 1) and the discrepancy between the two approaches increases, as the number of stories increases; in detail, an increment of about 45%, 47%, 42%, 49% and 48% is obtained, when  $n_f=4$ , for Type 1, 2, 3, 4 and 5, respectively.

Therefore, this solution is effective for potential use in areas of low and medium seismicity, where limited ductility demand is expected and, hence, stiffness rather than strength of such systems is crucial, particularly in the satisfaction of the building performance objectives for the immediate occupancy performance level or the serviceability limit state. Requirements for large lightly reinforced walls, belonging to medium ductility class, according to European rules (CEN 2005) are confirmed to be satisfied in case of multi-storey buildings, as already evidenced by shaking-table tests (Palermo *et al.* 2014) performed on prototypes similar to those numerically analyzed in this work. Such a consideration may thus serve as a reference for earthquake-resistant design and analysis of lightweight concrete bearing sandwich panels of similar type.

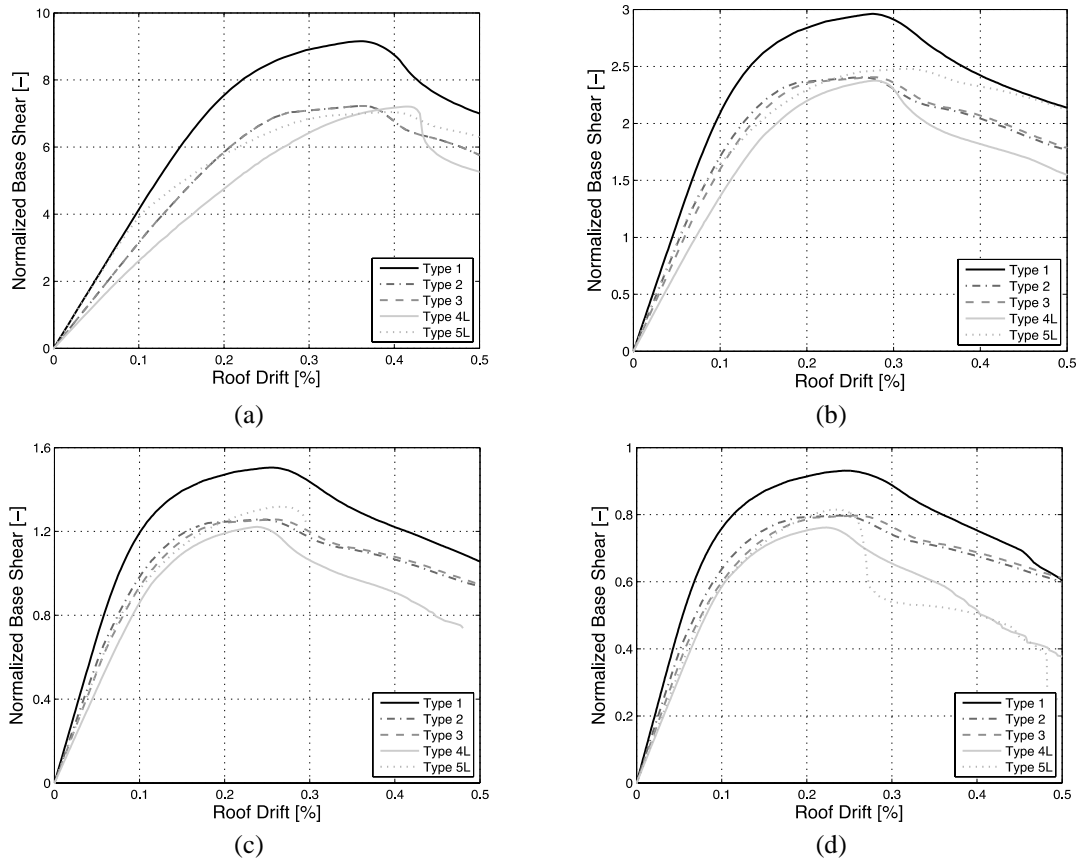


Fig. 15 Normalized base shear-roof drift curves for (a)  $n_f = 1$ ; (b)  $n_f = 2$ ; (c)  $n_f = 3$  and (d)  $n_f = 4$ , respectively

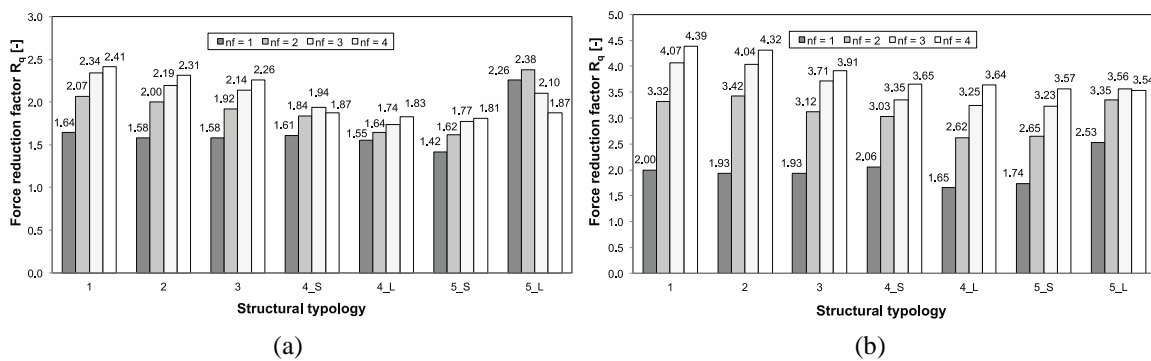


Fig. 16  $R_q$  estimates for each structural typology and height, assuming (a)  $\Delta_{peak}$  and (b)  $\Delta_{0.4\%}$ , respectively

## 5. Conclusions

The numerical research reported herein focuses on the seismic response assessment of lightweight lightly reinforced shotcrete sandwich panels, proposing a time saving mechanical

model, based on a combination of rigid Bernoulli beam and nonlinear multi-spring elements that equivalently include cyclic-related mechanisms, when performing nonlinear static monotonic analyses on such lateral-force resisting systems. This modeling procedure has been implemented, within an open source FE code, to reproduce the experimental response of full-scale specimens subjected to pseudo-static cyclic destructive tests selected from a past campaign (Pavese and Bournas 2011). A series of conventional displacement-controlled pushover analyses are then conducted on low- to mid-rise building prototypes representative of the construction technology investigated, aiming to quantify their FRFs, in accordance with a conventional methodology (Miranda and Bertero 1994). The prevailing observations and conclusions, drawn from this study, can be summarized as follows:

- The numerical idealization proposed appears a rational technique for simulating the seismic behaviour of such stocky walls at a global scale, since it consistently predicts their lateral load-bearing capacity:  $0.908 < R_r < 1.016$ , with average and standard deviation of 0.973 and 4%, respectively. By contrast, the mismatch between FE and experimental estimates increases, as the lateral displacement demand increases and major damage propagates into the panel.

- The sensitivity of peak base shear, as well as stiffness and strength degradation, to boundary conditions, axial load and geometry, in terms of both wall depth and presence of openings, has been quantified, showing a trend between the accuracy of numerical predictions and parametric changes in these quantities.

- The series of base shear-roof displacement capacity curves obtained for the reference layouts considered in this study reveal a trend between the addition of upper stories and the reduction in stiffness and lateral load-bearing capacity of these buildings, composed of a regular and industrialized construction scheme. Accordingly, the FRF is confirmed to increase, as the number of floors increases, particularly for regular structures.

- Even if this technology is in contrast with specific prescriptions for structural walls (e.g., material properties and wall thickness), the multi-storey buildings investigated herein provide satisfying values of  $R_q$ . Reserves close to those demanded by the current version of the European seismic Code (CEN 2005) for a large lightly reinforced wall system designed in medium ductility class are computed, whether 0.4% is fixed as a conventional drift target.

## Acknowledgments

The authors would like to express their gratitude to the company EMMEDUE for the financial support received through a one year framework programme established with the European Centre for Training and Research in Earthquake Engineering. The authors are deeply indebted to Dr. Marco Raimondi and Dr. Davide Bellotti for the extensive comments given on this research.

## References

- Antoniou, S. and Pinho, R. (2004), "Advantages and limitations of adaptive and non-adaptive force-based pushover procedures", *J. Earthq. Eng.*, **8**(4), 497-522.
- Arshian, A.H., Morgenthal, G. and Narayanan, S. (2016), "Influence of modelling strategies on uncertainty propagation in the alternate path mechanism of reinforced concrete framed structures", *Eng. Struct.*, **110**, 36-47.

- Belleri, A. and Riva, P. (2012), "Seismic performance and retrofit of precast grouted sleeve connections", *PCI J.*, **57**(1), 97-109.
- Belleri, A., Brunesi, E., Nascimbene, R., Pagani, M. and Riva, P. (2015), "Seismic performance of precast industrial facilities following major earthquakes in the Italian territory", *J. Perform. Constr. Fac.*, ASCE, **29**(5), 04014135.
- Beyer, K., Dazio, A. and Priestley, M.J.N. (2008), "Inelastic wide-column models for U-shaped reinforced concrete walls", *J. Earthq. Eng.*, **12**(S1), 1-33.
- Bruggi, M. (2009), "Generating strut-and-tie patterns for reinforced concrete structures using topology optimization", *Comput. Struct.*, **87**(23-24), 1483-1495.
- Brunesi, E., Bolognini, D. and Nascimbene, R. (2015a), "Evaluation of the shear capacity of precast-prestressed hollow core slabs: numerical and experimental comparisons", *Mater. Struct.*, **48**(5), 1503-1521.
- Brunesi, E., Nascimbene, R., Bolognini, D. and Bellotti, D. (2015b), "Experimental investigation of the cyclic response of reinforced precast concrete framed structures", *PCI J.*, **60**(2), 57-79.
- Brunesi, E., Nascimbene, R., Deyanova, M., Pagani, C. and Zambelli, S. (2015c), "Numerical simulation of hollow steel profiles for lightweight concrete sandwich panels", *Comput. Concrete*, **15**(6), 951-972.
- Brunesi, E. and Nascimbene, R. (2015), "Numerical web-shear strength assessment of precast prestressed hollow core slab units", *Eng. Struct.*, **102**, 13-30.
- Brunesi, E., Nascimbene, R. and Rassati, G.A. (2014), "Response of partially-restrained bolted beam-to-column connections under cyclic loads", *J. Constr. Steel. Res.*, **97**, 24-38.
- Brunesi, E., Nascimbene, R. and Rassati, G.A. (2015d), "Seismic response of MRFs with partially-restrained bolted beam-to-column connections through FE analyses", *J. Constr. Steel. Res.*, **107**, 37-49.
- Brunesi, E. and Nascimbene, R. (2014), "Extreme response of reinforced concrete buildings through fiber force-based finite element analysis", *Eng. Struct.*, **69**, 206-215.
- Brunesi, E., Nascimbene, R., Parisi, F. and Augenti, N. (2015e), "Progressive collapse fragility of reinforced concrete framed structures through incremental dynamic analysis", *Eng. Struct.*, **104**, 65-79.
- Brunesi, E., Nascimbene, R. and Parisi, F. (2016), "Progressive collapse fragility models of RC framed buildings based on pushdown analysis", *Proceedings of the VII European Congress on Computational Methods in Applied Sciences and Engineering*, Crete Island, Greece, June.
- CEN, European Committee for Standardization (2005), "*EN 1998-1-5. Eurocode 8: design of structures for earthquake resistance - Part 1.5: specific rules for concrete buildings*", Brussels, Belgium.
- Chang, G.A. and Mander, J.B. (1994), "*Seismic energy based fatigue damage analysis of bridge columns: Part 1 - Evaluation of seismic capacity*", NCEER Technical Report No. NCEER-94-0006, State University of New York, Buffalo, NY.
- Chopra, A.K. and Goel, R.K. (2002), "A modal pushover analysis procedure for estimating seismic demands for buildings", *Earthq. Eng. Struct. Dyn.*, **31**(3), 561-582.
- Colotti, V. (1993), "Shear behavior of RC structural walls", *J. Struct. Eng.*, ASCE, **119**(3), 728-746.
- Dazio, A., Beyer, K. and Bachmann, H. (2009), "Quasi-static cyclic tests and plastic hinge analysis of RC structural walls", *Eng. Struct.*, **31**(7), 1556-1571.
- Fajfar, P. (2000), "A nonlinear analysis method for performance based seismic design", *Earthq. Spectra*, **16**(3), 573-592.
- Ghobarah, A. and Youssef, M. (1999), "Modelling of reinforced concrete structural walls", *Eng. Struct.*, **21**(10), 912-923.
- Hidalgo, P.A., Ledezma, C.A. and Jordan, R.M. (2002), "Seismic behavior of squat reinforced concrete shear walls", *Earthq. Spectra*, **18**(2), 287-308.
- Hung, C.-C. and El-Tawil, S. (2010), "Hybrid rotating/fixed-crack model for high performance fiber reinforced cementitious composites", *ACI Mater. J.*, **107**(6), 569-577.
- Kim, S. and D'Amore, E. (1999), "Pushover analysis procedure in earthquake engineering", *Earthq. Spectra*, **15**(3), 417-434.
- Krawinkler, H. and Seneviratna, G.D.P.K. (1998), "Pros and cons of a pushover analysis of seismic performance evaluation", *Eng. Struct.*, **20**(4-6), 452-462.

- Kurama, Y.C. (2000), "Seismic design of unbonded post-tensioned precast concrete walls with supplemental viscous damping", *ACI Struct. J.*, **97**(4), 648-658.
- Kurama, Y.C., Sause, R., Pessiki, S. and Lu, W.L. (1999), "Lateral load behaviour and seismic design of unbonded post-tensioned precast concrete walls", *ACI Struct. J.*, **96**(4), 622-632.
- Mander, J.B., Priestley, M.J.N. and Park, R. (1988), "Theoretical stress-strain model for confined concrete", *J. Struct. Eng.*, ASCE, **114**(8), 1804-1826.
- McKenna, F., Fenves, G.L. and Scott, M.H. (2015), *OpenSees - Open system for earthquake engineering simulation*, Pacific Earthquake Engineering Research Center, University of California, Berkeley, CA. (<http://opensees.berkeley.edu>) (last accessed: March 2015).
- Miao, Z.W., Lu, X.Z., Jiang, J.J. and Ye, L.P. (2006), "Nonlinear FE model for RC shear walls based on multi-layer shell element and microplane constitutive model", *Proceedings of Computational Methods in Engineering and ScienceX*, Sanya, Hainan, China, August.
- Miranda, E. and Bertero, V.V. (1994), "Evaluation of strength reduction factors for earthquake-resistant design", *Earthq. Spectra*, **10**(2), 357-379.
- Mousavi, S.A., Zahrai, S.M. and Bahrami-Rad, A. (2014), "Quasi-static cyclic tests on super-lightweight EPS concrete shear walls", *Eng. Struct.*, **65**, 62-75.
- Nascimbene, R. (2014), "Towards non-standard numerical modeling of thin-shell structures: geometrically linear formulation", *Int. J. Comput. Meth. Eng. Sci. Mech.*, **15**(2), 126-141.
- Nascimbene, R. and Venini, P. (2002), "A new locking-free equilibrium mixed element for plane elasticity with continuous displacement interpolation", *Comput. Meth. Appl. Mech. Eng.*, **191**(17-18), 1843-1860.
- Orakcal, K., Wallace, J.W. and Conte, J.P. (2004), "Flexural modeling of reinforced concrete walls-model attributes", *ACI Struct. J.*, **101**(5), 688-698.
- Orakcal, K., Massone, L.M. and Wallace, J.W. (2009), "Shear strength of lightly reinforced wall piers and spandrels", *ACI Struct. J.*, **106**(4), 455-465.
- Palermo, M., Gil-Martin, L.M., Trombetti, T. and Hernandez-Montes, E. (2013), "In-plane shear behaviour of thin low reinforced concrete panels for earthquake reconstruction", *Mater. Struct.*, **46**(5), 841-856.
- Palermo, M., Ricci, I., Silvestri, S., Gasparini, G., Trombetti, T., Foti, D. and Ivorra, S. (2014), "Preliminary interpretation of shaking-table response of a full-scale 3-storey building composed of thin reinforced concrete sandwich walls", *Eng. Struct.*, **76**, 75-89.
- Palermo, M. and Trombetti, T. (2016), "Experimentally-validated modelling of thin RC sandwich walls subjected to seismic loads", *Eng. Struct.*, **119**, 95-109.
- Pavese, A. and Bournas, D.A. (2011), "Experimental assessment of the seismic performance of a prefabricated concrete structural wall system", *Eng. Struct.*, **33**(6), 2049-2062.
- Pecce, M., Ceroni, F., Bibbò, F.A. and De Angelis, A. (2014), "Behaviour of RC buildings with large lightly reinforced walls along the perimeter", *Eng. Struct.*, **73**, 39-53.
- Pennucci, D., Calvi, G.M. and Sullivan, T.J. (2009), "Displacement based design of precast walls with additional dampers", *J. Earthq. Eng.*, **13**(S1), 40-65.
- Priestley, M.J.N., Sritharan, S.S., Conley, J.R. and Pampanin, S. (1999), "Preliminary results and conclusions from the PRESSS five-story precast concrete test building", *PCI J.*, **44**(6), 42-67.
- Priestley, M.J.N., Verma, R. and Xiao, Y. (1994), "Seismic shear strength of reinforced concrete columns", *J. Struct. Eng.*, ASCE, **120**(8), 2310-2329.
- Rezaifar, O., Kabir, M.Z., Taribakhsh, M. and Tehranian, A. (2008), "Dynamic behaviour of 3D panel single-storey system using shaking-table testing", *Eng. Struct.*, **30**(2), 318-337.
- Ricci, I., Palermo, M., Gasparini, G., Silvestri, S. and Trombetti, T. (2013), "Results of pseudo-static tests with cyclic horizontal load on cast in situ sandwich squat concrete walls", *Eng. Struct.*, **54**, 131-149.
- Saad, G., Najjara, S. and Saddik, F. (2016), "Seismic performance of reinforced concrete shear wall buildings with underground stories", *Earthq. Struct.*, **10**(4), 965-988.
- Salonikios, T.N., Kappos, A.J., Tegos, I.A. and Penelis, G.G. (1999), "Cyclic load behavior of low-slenderness R/C walls: design basis and test results", *ACI Struct. J.*, **96**(4), 649-660.
- Salonikios, T.N., Kappos, A.J., Tegos, I.A. and Penelis, G.G. (2000), "Cyclic load behavior of low-slenderness R/C walls: failure modes, strength and deformation analysis, and design implications", *ACI*

- Struct. J.*, **97**(1), 132-141.
- Werasak, R. and Jing, M. (2009), "Analysis modelling of seismic behaviour of lightweight concrete shear walls", *Proceedings of the International Multiconference of Engineers and Computer Scientists*, Hong Kong, March.
- Zygouris, N.S., Kotsovos, G.M. and Kotsovos, M.D. (2015), "Design for earthquake-resistant short RC structural walls", *Earthq. Struct.*, **8**(3), 713-732.

SA